

Article

Preliminary Experimental Results and Modelling Study of Olive Kernel Gasification in a 2 MWth BFB Gasifier

Athanasios Lampropoulos ^{1,*}, Idoia Goñi Zubillaga ², Raúl Pérez-Vega ², Nikolaos Ntavos ³, Yannis Fallas ³ and Georgios Varvoutis ^{1,*}

¹ Department of Mechanical Engineering, University of Western Macedonia, 50100 Kozani, Greece

² Biomass Department, National Renewable Energy Centre (CENER), 31621 Sarriguren, Spain

³ Cluster of Bioeconomy and Environment of Western Macedonia, 50100 Kozani, Greece

* Correspondence: alabropoulos@uowm.gr (A.L.); gvarvoutis@uowm.gr (G.V.)

Abstract: Gasification is a promising and attractive thermochemical method for biomass-to-energy conversion, with fluidized bed reactors being one of the best options for large-scale operations. Olive residues in particular are potentially excellent candidate biomass fuels in the Mediterranean area, due to the region's increased capacity in olive oil production. Herein, the gasification experiments of olive kernels in a 2 MWth air-blown, bubbling fluidized bed reactor located at CENER's facilities (BIO2C) in Navarra, Spain are presented. Even though technical issues were demonstrated due to the operation of the plant with a high-density biomass fuel and given the scale of the process, a quasi-steady-state and isothermal 12 h operation at an equivalence ratio of 0.25 ± 0.03 was attained. Given the satisfactory experimental results, an Aspen Plus simulation model of the process was also attempted. Notably, the proposed methodology agrees well with the experimental results and can be regarded as a starting point in future studies examining the gasification of relevant biomass in a MW-scale unit. Next, the effect of equivalence ratio and residual biomass moisture content were also evaluated, with the scope of designing future experiments that require minor modifications in the already existing apparatus. Finally, a syngas utilization route through the provision of energy for district heating purposes in the nearby village of Aoiz was proposed.

Keywords: olive kernel; biomass gasification; bubbling fluidized bed; aspen plus; syngas to district heating



Citation: Lampropoulos, A.; Zubillaga, I.G.; Pérez-Vega, R.; Ntavos, N.; Fallas, Y.; Varvoutis, G. Preliminary Experimental Results and Modelling Study of Olive Kernel Gasification in a 2 MWth BFB Gasifier. *Processes* **2022**, *10*, 2020. <https://doi.org/10.3390/pr10102020>

Academic Editors: Zhien Zhang and Zacharias Frontistis

Received: 5 September 2022

Accepted: 24 September 2022

Published: 7 October 2022

Publisher's Note: MDPI stays neutral with regard to jurisdictional claims in published maps and institutional affiliations.



Copyright: © 2022 by the authors. Licensee MDPI, Basel, Switzerland. This article is an open access article distributed under the terms and conditions of the Creative Commons Attribution (CC BY) license (<https://creativecommons.org/licenses/by/4.0/>).

1. Introduction

The European Commission launched the Green Deal initiative in December 2019, intending to meet the ambitious goal of climate neutrality and economic growth without the need for fossil fuel consumption [1–3]. Towards this direction, the increase of renewable's share in the gross energy consumption and the adoption of circular economy principles through innovative and efficient processes constitute important measures towards achieving a clean energy transition. In this regard, biomass is a cheap, widely distributed and renewable energy source associated with a neutral carbon footprint [4–7]. Furthermore, in a potential biomass-based system equipped with a CO₂ capture system, negative CO₂ emissions can be achieved, with an estimated potential of CO₂ sequestration ranging between 2.2–12.0 Gt CO₂ by 2050 [8]. Bioenergy potential in the EU is estimated to contribute 140 Mtoe to the gross final energy consumption (GFEC) in 2022. For the target year of 2030, bioenergy capacity could reach values between 160 and 180 Mtoe, representing a share of around 15% of the GFEC [9]. Additionally, bioelectricity generation in the EU-28 countries for the period 2019–2020 amounted to ca. 160 TWh [10].

However, considering the cases of Spain and Greece, these two Mediterranean countries contributed only a relatively low portion in the EU total bioelectricity production in the year 2019, generating ca. 5.0 and 0.4 TWh, respectively [10]. This finding is somewhat oxymoronic, considering their rather high biomass utilization potential compared

to most of the European Union countries. In particular, Greece generates a large amount of agricultural and agro-industrial residues, equal to approximately 23 Mtonnes, being the third largest olive oil industry worldwide, with an annual capacity of approximately 350 ktonnes of olive oil [11–14]. As a consequence, residues from the olive oil production industry constitute half of the total agricultural and agro-industrial residues (Figure 1). Similarly, Spain is the second largest olive oil industry with an average annual production of 1.4 Mtonnes of olive oil (Figure 2). It can be seen that a slight increase in olive oil production has been demonstrated in the latest years, which in turn is associated with a greater increase in the absolute amount of olive residues. This is a direct result of the olive oil extraction process itself, as described in the next paragraph. Also, as in Greece, olive residues represent a great share among other agro-industrial residues, with an annual quantity of ca. 9.5 Mtonnes (2020 data) [11].

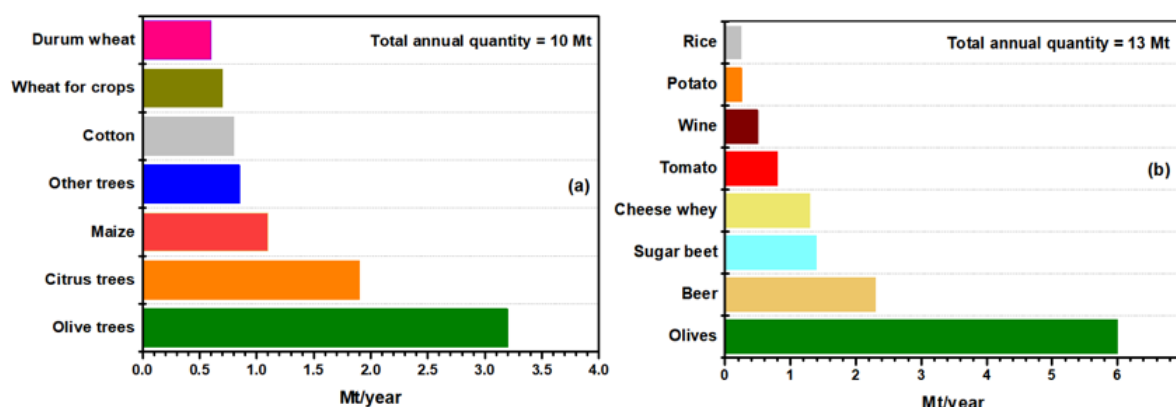


Figure 1. Agricultural (a) and agro-industrial (b) residues capacity in Greece.

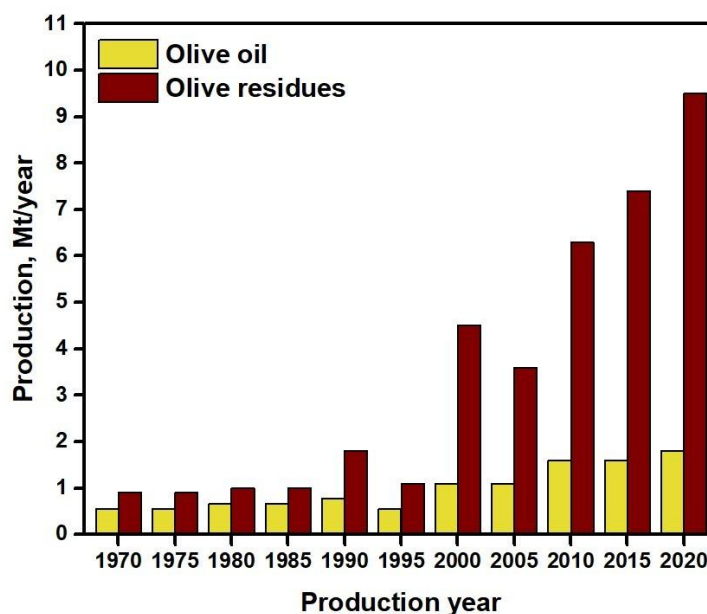


Figure 2. Annual production of olive oil and olive residues in Spain in the last 50 years.

Indeed, the olive oil industry can potentially serve as an excellent source for the bioenergy utilization sector, as it generates a wide array of wastes and by-products with variable characteristics, a further breakdown of which is schematically depicted in Figure 3. In any case, their rate of production and physicochemical properties largely depend on the oil extraction method. Typically, a small portion of these by-products (mostly olive kernel) is combusted in order to meet industrial heating demands. However, based on a typical

olive oil two-phase extraction process, only 1/5 of the olive fruit (i.e., 200 kg, based on 1 tonne) is eventually converted to virgin olive oil. The remaining quantity corresponds to ca. 620 kg of olive pomace, 100 kg olive of kernel/pit/stone and 80 kg of leaves and twigs. Olive pruning represent another abundant source of residues, corresponding to approximately 6 tonne/ha per annum [15–17].

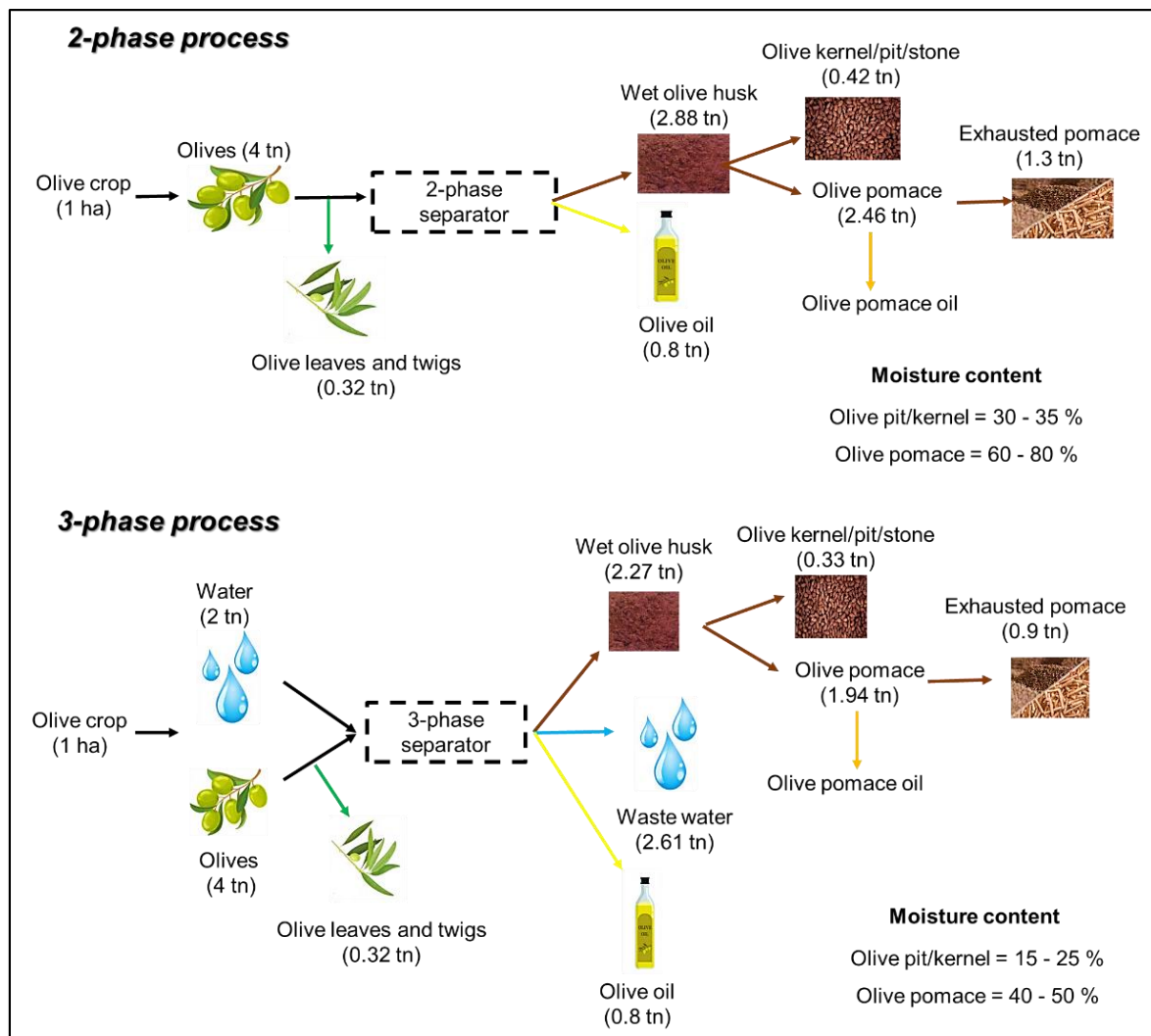


Figure 3. Two- and three-phase olive oil extraction process.

In practice, there exist several processes for the conversion of biomass and the development of high-efficient and low-cost renewable energy power plants. In this regard, one of the most effective and widely used biomass conversion routes is gasification, which is a thermo-chemical process that transforms the solid biomass into a gaseous energy carrier. Biomass gasification typically takes place at high temperatures (600–1000 °C) and atmospheric pressure by employing several gasifying agents as the gaseous feed (i.e., air or pure oxygen and/or steam and/or CO₂), resulting in an outlet gas mixture containing mainly H₂, CO, CO₂, CH₄ and traces of light hydrocarbons, commonly referred to as synthesis gas or syngas. The produced syngas is a very versatile product that can be utilized downstream either as fuel in internal combustion engines, in gas turbines, in high-temperature solid oxide fuel cells (SOFCs) or as raw material in the Fischer-Tropsch process for the production of synthetic liquid fuels and value-added chemicals [18–22]. From a process system perspective, the main factors affecting syngas quality (that is, its composition and in turn its heating value) are the employed gasifying agent(s), operating temperature and pressure,

gasifier design and heating mode, addition of catalysts, and feedstock composition. In Table 1, a summary of the main advantages and drawbacks of the implementation of different gasifying agent(s) is presented.

Specifically, steam and/or oxygen gasification leads to a N₂-free syngas with a relatively high heating value (10–20 MJ/Nm³), suitable for several downstream processes such as high-efficient power generation via combined gasification-SOFC cycles and biomass conversion to high added-value products such as hydrocarbons, methanol or dimethyl ether [23–25]. The employment of air as an economical and highly abundant gasifying agent results in a syngas that is characterized by a significantly low heating value (~5 MJ/Nm³) due to the inevitably high nitrogen content (40–50% on a volume basis), limiting its application in the power generation sector [26–29]. Moreover, the usage of pure CO₂ as a gasification agent can be employed as a means of CO₂ emissions mitigation via flue gas recycling. Equally important, syngas produced by the CO₂ gasification process is characterized by a high heating value (10–15 MJ/Nm³), though the progression of the Boudouard reaction which enhances CO production (Equation (1)). However, the main drawback of steam and/or CO₂ biomass gasification is the need for external heat provision in order to maintain the high gasification temperature, as well as the need for a relatively pure CO₂ stream in the case of CO₂ gasification [30].

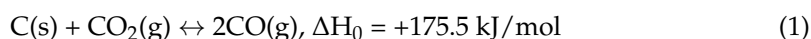


Table 1. Advantages and disadvantages of various gasification agents [31,32].

Gasifying Agent	Advantages	Disadvantages
Air	<ul style="list-style-type: none"> ✓ Heat generation from combustion ✓ Low/moderate char and tar content ✓ Inexpensive 	<ul style="list-style-type: none"> ✗ Low heating value (4–7 MJ/Nm³) ✗ N₂ dilution
O ₂	<ul style="list-style-type: none"> ✓ N₂-free syngas ✓ High heating value (10–20 MJ/Nm³) 	<ul style="list-style-type: none"> ✗ Cost-intensive
H ₂ O	<ul style="list-style-type: none"> ✓ High heating value (10–18 MJ/Nm³) ✓ H₂-rich syngas ✓ N₂-free syngas 	<ul style="list-style-type: none"> ✗ Very endothermic ✗ Relatively low CO concentration
CO ₂	<ul style="list-style-type: none"> ✓ Moderate heating value (10–15 MJ/Nm³) ✓ High CO and low CO₂ content 	<ul style="list-style-type: none"> ✗ Very endothermic ✗ Low H₂ concentration

Different approaches and gasifier designs have been extensively examined in the literature, with Table 2 summarizing the main characteristics of the conventional air-gasification technologies, i.e., downdraft, updraft, bubbling fluidized bed (BFB) and circulating fluidized bed (CFB). Fixed bed and fluidized bed gasifiers are usually implemented in biomass gasification power plants [33–35]. Fixed bed gasifiers (updraft and downdraft) are a more robust technology that is commonly used in small-scale gasification power plants and are characterized by a low tar content, simple construction and reliable operation. However, their low flexibility towards handling heterogeneous raw materials, along with their inability to exploit high-moisture biomass fuels may sometimes be a limiting factor for their implementation [33,35]. Concerning the syngas LHV value in the case of updraft and downdraft gasifiers, in the former case, solid biomass is counter-current to the gasifying agent, thus the produced syngas immediately flows to the lower-temperature part of the reactor after its formation, leading to decreased cracking of tar compounds into gases, which further lowers the LHV. Nonetheless, in air-blown fixed-bed gasification, the LHV of the generated syngas is practically the same in either updraft or downdraft conditions and there is more often than not an overlap between the LHV values, thus a direct comparison

between the two configurations cannot always be applied [36,37]. On the contrary, fluidized bed gasifiers are the simplest gasifier design and can be implemented at a higher scale, since they are associated with a satisfactory gas-solid contact due to the existing fluidizing conditions inside the reactor [22,38–43]. Typically, the gasification process in BFB gasifiers takes place in three linked zones including drying and devolatilization, partial oxidation of the as-produced volatiles and char, and finally reforming reactions and char gasification.

Table 2. General characteristics of conventional air gasification technologies.

Gasification Parameter	Gasifier Type			
	Downdraft	Updraft	BFB	CFB
Pressure (bar)	1	1	1.35	1.19
Temperature (°C)	700–1200	700–900	650–950	800–1000
LHV (MJ/Nm ³)	5–6	4.5–5	4–7.5	4–7.5
Thermal input (MWth)	<5	<20	3–100	20–100
Tar content (g/Nm ³)	0.015–0.5	30–150	1–50	1–30
Particulates	Low	Low	Very low (cyclone)	
Particle size (mm)	20–100	5–100	10–100	
Moisture (wt.%)	<15	<50	<40	
Ash (wt.%, d.b.)	<5	<15	<20	
Morphology	Uniform	Uniform	Uniform	
Density (kg/m ³)	>500	>400	>100	

The oxidative gasifying agent, which acts also as a fluidizing agent, is the driving force which can transfer a solid carbon species into the gaseous phase, as biomass carrying oxygen and hydrogen is not sufficient for the partial oxidation of char and volatiles. In some cases, an over-stoichiometric amount of air is supplied in the reactor in order to shift the equilibrium of the oxidation reactions towards oxygen consumption. In this way, the high exothermicity of the involved reactions releases significant amounts of heat that can be utilized by the system in order to reach and maintain the high temperatures required for the endothermic reforming and gasification reactions. In practice, typical equivalence ratio (ER) values reported in the literature for BFB reactors [38,40,42] are between 0.2 and 0.4. A higher ER value is inevitably associated with an increased N₂ dilution of the generated syngas, due to the increased air influx and in turn the heating value of the final gas being lowered. Ergo, a balance between the need for heat generation for the endothermic reactions induced by increased air flow and the detrimental effect of increased N₂ content in the heating value must almost always be attained.

A schematic representation of a typical bubbling fluidized bed reactor is illustrated in Figure 4, along with its main operational characteristics. According to the gas-solid fluidization principle, the interaction of the solid fuel with the inert bed material improves the rheological characteristics of the bed, especially upon contact with the gaseous agent. Typically, the bed material consists of granular solid particles that act as heat carriers placed at the bottom of the reactor. Besides providing the demanded process oxygen, the gasifying agent also serves as a fluidized medium. Therefore, it is supplied at the bottom of the reactor (e.g., through a plenum chamber) with an appropriate flow rate that induces the desired fluidization level to expand the static bed up to a suitable volume. This allows the dense zone of the bed to be formed at the bottom of reactor, where biomass is usually fed just above the distributor plate by which gas is supplied. Selecting this fed point could improve both the heat transfer from solid particles to biomass and the carbon/char conversion efficiency due to the high degree of solid-solid mixing. Nevertheless, BFB reactors are characterized by relatively low gasification efficiency, ascribed to the mentioned entrainment and elutriation of small char particles [39,42]. In any case, process efficiencies in biomass gasification on BFB reactors are dependent on a variety of parameters and should be evaluated in a case-specific manner [33,39,44]

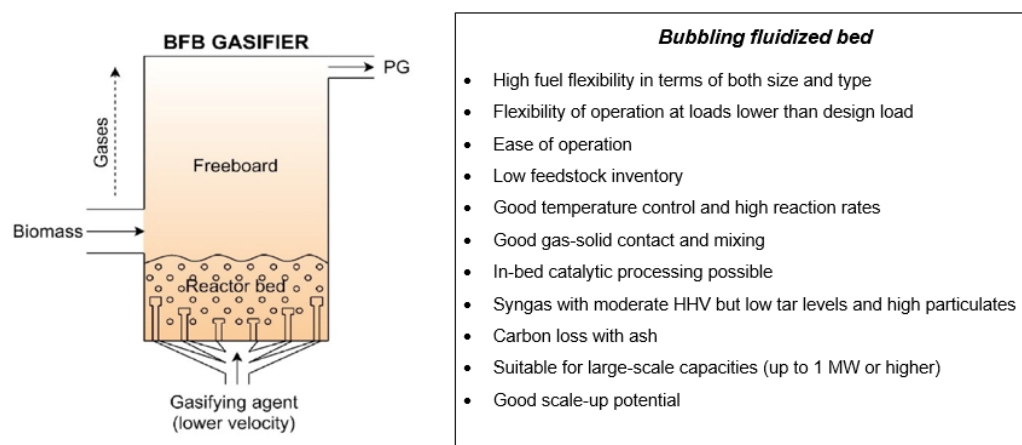


Figure 4. Schematic representation and features of a BFB gasifier. Reproduced with permission from Elsevier [34].

Silica sand is the most commonly used bed material due to its abundance and low price [45,46]. However, other solids with particular catalytic activity, such as olivine, limestone, dolomite and bauxite can induce the cracking of tar compounds in a quasi-catalytic manner, thus leading to a decreased tar concentration and in turn to an enhanced syngas quality [45–49]. Generally, in applying varying gasifying agents, a specific bed material can exert several main effects on the conversion of the biomass fuel. These effects can be categorized as; (i) a thermal effect, with fuel conversion induced by heat as well as the gasifying agent, (ii) a catalytic effect of the bed material, with specific metal species being present in the bed material acting as inherent catalysts, (iii) a catalysis by ash-forming elements, referring to the catalyzed tar reactions and steam gasification of char by the alkali and alkali metal-containing ash and (iv) an effect of oxygen transport, in essence referring to the increased mobility of oxygen species from the combustor to the gasifier and their participation in reduction/oxidation loops [46,48].

However, there are several factors that affect the tar cracking efficiency of the different bed materials. For instance, bauxite acts as an alkali-binding material commonly used in coupled combustion and gasification units. Alkali species contained in the biomass ash are physically absorbed to bauxite in the combustion zone, whereas they can be released in the gasification zone, influencing the quality of the produced syngas. In other words, the alkali-releasing ability of bauxite under a gasification environment increases the char gasification rate [46,48]. Additionally, bauxite, despite its low Fe content, attains significant oxygen transport capabilities, which can be attributed in part to the ash load of the material [46].

Concerning the large-scale implementation of olive residues as a source of biomass gasification in power plants, there is a limited number of studies concerning the exploitation of olive kernel and/or olive pit residues in various gasification cycles combined with downstream processes for power generation [26–29,50]. For instance, Vera et al. [26,28] examined the air gasification of olive pit residues (100 kg/h) in a fixed-bed downdraft gasifier coupled with a gas engine at an equivalence ratio of 0.2 at 1000 °C. The experimental results showed satisfactory cold gas efficiency (in the range of 71–76%) and a relatively high (on the basis of using air as a gasifying agent) syngas LHV for both feedstocks, namely 4.8 and 5.4 MJ/kg. To the best of the authors understanding, only two studies have investigated the air-blown gasification of olive kernels in a BFB reactor [29,51]. Specifically, Michailos et al. [51] investigated the effect of different operational conditions in a 5 kW pilot-scale BFB gasifier exploiting 1 kg/h of olive kernels. The authors validated the experimental results with a proposed simulation in Aspen Plus software. They concluded that the optimum operational conditions were, ER = 0.2 and T = 750 °C. At these conditions, the concentration of H₂+CO and the LHV of the produced syngas was ca. 42% and 6.7 MJ/Nm³, respectively. Most of the results obtained from the proposed simulation model were in good agreement with their experimental work. Elsewhere, Manara et al, [29] conducted a

similar study based on the previous work by Michailos et al., investigating the economic, environmental and social impacts of a potential scale-up of a 5 kW air-blown BFB reactor. They highlighted the potential benefits of the symbiosis of a small-scale gasification power plant with agricultural associations and processing companies towards meeting heating and electrical demands, in conjunction with additional benefits of zero-cost logistics in terms of feedstock provision.

Collectively and to the best of our knowledge, there exists no study investigating the exploitation of olive kernel residues in a MW-scale gasification unit through the combination of experimental and theoretical simulation results. In light of the above, in the present work the operation of a 2 MWth gasification large scale plant using olive kernel biomass fuel is firstly presented. The gasification experiments were conducted at the CENER facilities (BIO2C) in Navarra (<https://www.bio2c.es/>, accessed on 4 September 2022), Spain at an air-blown bubbling fluidized bed reactor with bauxite as the bed material. Despite the technical issues derived from the first-time operation of the plant with high-density biomass fuel and given the scale of the process, a quasi-steady-state and isothermal 12 h operation of air gasification at an ER of 0.25 ± 0.03 was established. Motivated by the satisfactory experimental results, a simulation of the process was next attempted in Aspen Plus software based on experimental data and relevant literature. Notably, the proposed simulation methodology is in good agreement with the experimental results and can be employed as a starting point in future studies examining the more elaborate simulation of MW-scale gasification of relevant biomass fuels. With this, the effect of equivalence ratio and residual biomass moisture content were assessed in a relatively accurate manner, with the scope of designing future olive kernel gasification experiments that require minor modifications in the already existing apparatus. Lastly, a brief assessment of the possible exploitation of the generated syngas for district heating purposes was attempted.

2. Materials and Methods

2.1. Characterization of Olive Kernel and Bauxite

The necessary olive kernel quantity was provided by local suppliers and was stored on-site. Subsequently, olive kernels were characterized in terms of ultimate/proximate analysis, low heating value (LHV), bulk density, particle size distribution (Table 3) and thermogravimetric analysis. Typical values of carbon, oxygen and hydrogen were obtained in comparison to other olive kernel fuels [26,28], while negligible quantities of nitrogen, sulfur and chlorine were measured. The high moisture content of the as-received olive kernels was attributed to the absence of pre-drying. Finally, the heating value of the biomass lies on the mean value of other lignocellulosic biomass fuels [52].

Table 3. Properties of the raw olive kernel.

Ultimate Analysis (wt.% d.a.f.)			Immediate Analysis (wt.%)						
C	O	H	N	H ₂ O	Ash ^{d.b.}	LHV ^{w.b.} (MJ/kg)	LHV ^{d.b.} (MJ/kg)	LHV ^{d.a.f.} (MJ/kg)	Bulk Density (kg/m ³)
50.9	43.0	6.0	0.1	16.8	0.6	15.3	18.9	19.0	730

d.a.f.: dry ash-free, d.b.: dry basis, w.b.: wet basis.

Also, the particle size distribution of the as-received olive kernels was determined by granulometric analysis, and the results are shown in Figure S1. It can be clearly seen that the particle size of the olive kernel fuel was in the range 2.0–3.5 mm, which is suitable for exploitation in the existing air-blown BFB gasifier.

The thermal decomposition of the as-received olive kernel fuel was assessed in a typical macro-TG apparatus by loading ca. 1.20 g in the TG analyzer. Experiments were conducted under air flow (2 L/min) in the temperature regime of 25–1000 °C [53] at a heating rate of 10 K/min. Bauxite (type RASC) was used as a bed material. A total of

1300 kg of bauxite particles were introduced into the gasifier, the physicochemical properties of which can be seen in Table S1.

2.2. Pilot Plant Description

The gasification of olive kernels was conducted in the gasification unit at the Biorefinery and BioEnergy Centre (BIO2C) of the Spanish National Renewable Energy Centre (CENER) in Aoiz, Navarra, Spain. The exact location and a general overview of the plant can be seen in Figures 5 and 6a, respectively. The unit is able to handle a wide range of operating parameters and a variety of biomass feed types and bed materials, as seen in Table 4. The designed nominal thermal power of the pilot plant is 2 MW, but is able to operate under nominal powers between 1.2–2.2 MWth with biomasses with a wide bulk density range covering an order of magnitude (i.e., between 80 and 800 kg/m³) and a moisture content of up to 30 wt.%.



Figure 5. Location of the gasification plant.

Table 4. Technical characteristics of the gasification plant.

Process Data	
Reactor Type	Atmospheric Bubbling Fluidized Bed (ABFB)
Nominal power (MWth)	2.0
Minimum power (MWth)	1.2
Operating pressure (barg)	0.3
Bed temperature (°C)	650–950
Freeboard temperature (°C)	700–1000
Inertization/purge gas	CO ₂
Biomass feed specifications	
Bulk density (kg/m ³)	80–800
Moisture content (%)	<30
Particle size (mm)	<30
Volatile matter (% d.a.f.)	68–87
Ash (% d.b.)	<13
Lower heating value (MJ/kg d.b.)	15.3–20.8
Bed material specifications	
Bulk density (kg/m ³)	1000–5000
Particle size (mm)	<1
Minimum fluidization velocity (m/s)	0.17
Fluidization velocity ratio	<2

d.b.: dry basis. d.a.f.: dry ash-free.

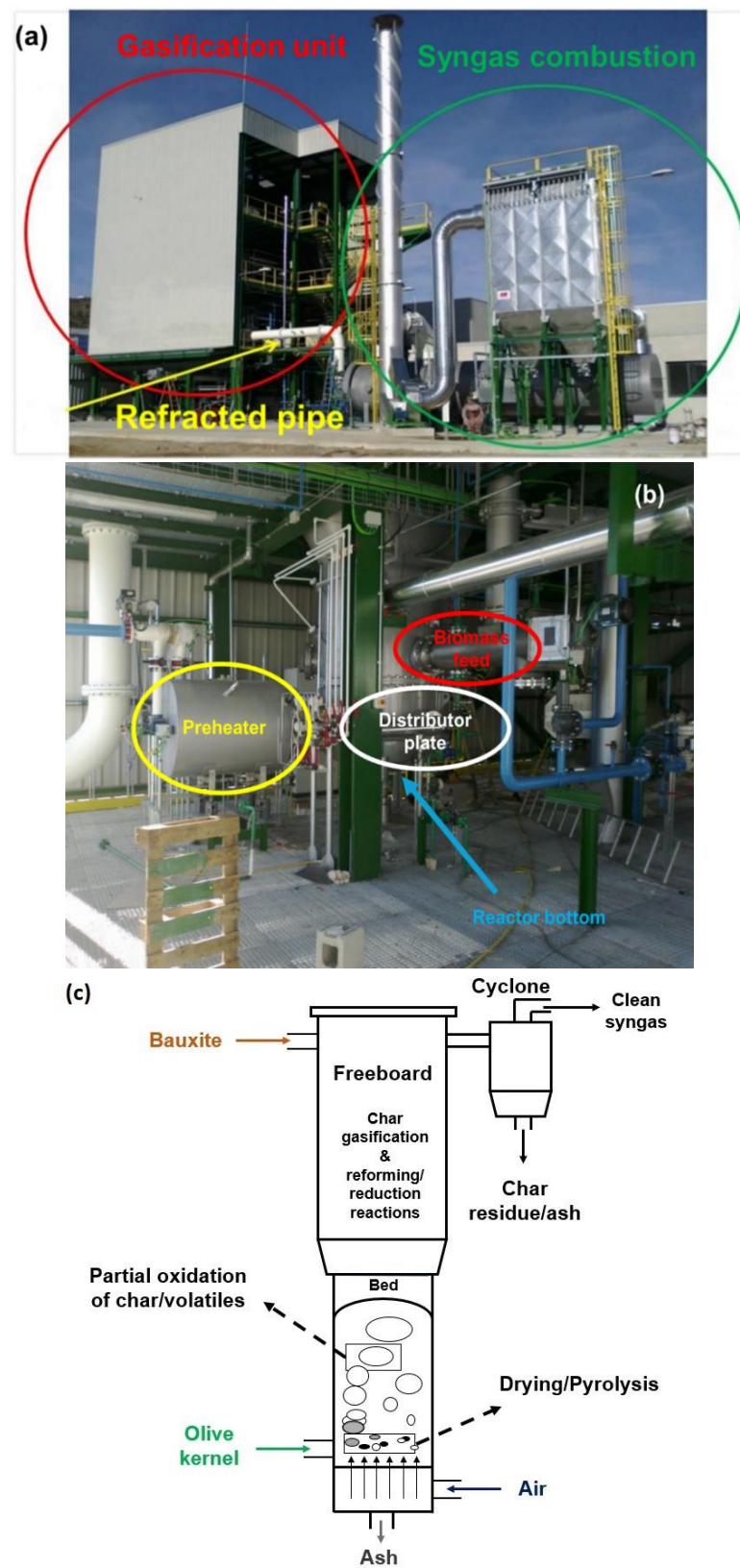


Figure 6. (a) General view of the gasification pilot plant, (b) the bottom part and (c) schematic representation of the BFB gasifier at BIO2C (adapted from [54]).

In general, the integrated plant is comprised of the following sub-units:

- Biomass feeding system

- Air-blown, atmospheric bubbling fluidized bed (ABFB) gasifier
- Syngas cleaning and discharge system
- Syngas combustion, flue gas cooling and cleaning system
- Distributed control system for remote and automatic operation (SCADA)
- Micro gas chromatograph (μ -GC) for gas analysis

The bottom part of the BFB gasifier along with identification of the main parts is shown in Figure 6b, whereas its schematic representation is shown in Figure 6c. The air is blown upward through a distributor plate to keep the bed particles in a state of suspension [54]. The solid biomass fuel is introduced at the bottom of the reactor, just above the distributor plate, and is rapidly mixed with the bed material, followed by intensified mass and heat transfer. The overall gasification takes place in three linked zones. Initially, drying of olive kernels upon heat exposure leads to moisture evaporation. Subsequently, the devolatilization process involving a series of complex reactions takes place, thus generating char, tars, light gases (H_2 , CO, CO_2 , CH_4 , H_2O), and other heavier hydrocarbons. The produced char, tar as well as H_2 and CO are then partially oxidized, a process that releases a large amount of heat that could be used to sustain the thermally-intensive and endothermic gasification reactions. Finally, in the freeboard zone, the products of partial combustion and uncombusted cracked pyrolysis products (volatiles, char) now pass to the freeboard/dilute/reduction zone where the reduction reactions take place [27]. Further gasification and/or reforming reactions (Boudouard reaction, water-gas shift reaction, etc.) occur, resulting in syngas generation.

2.3. Simulation Methodology

The general model used for the process simulation was based on the procedure followed by Grimekis et al. [55,56] as well as the general considerations reported in the review by Ajourloo et al. [32], and is illustrated in Figure 7. Specifically, the raw biomass (RAWOK) is initially decomposed in an RYield block, where it is converted from a non-conventional solid to its constituent conventional compounds (i.e., C, H_2 , N_2 , S, O_2 , and H_2O) as well as ash, according to the ultimate analysis of the solid (stream OK). In particular, ash was considered a non-conventional substance, char and solid carbon were both modelled as graphitic carbon, while all other compounds were considered as conventional compounds from the Aspen Plus database. Typically, for the proper definition of biomass, HCOALGEN and DCOALIGT models were employed for the calculations of enthalpy and density, respectively and Peng-Robinson was selected as the method for thermophysical properties calculation.

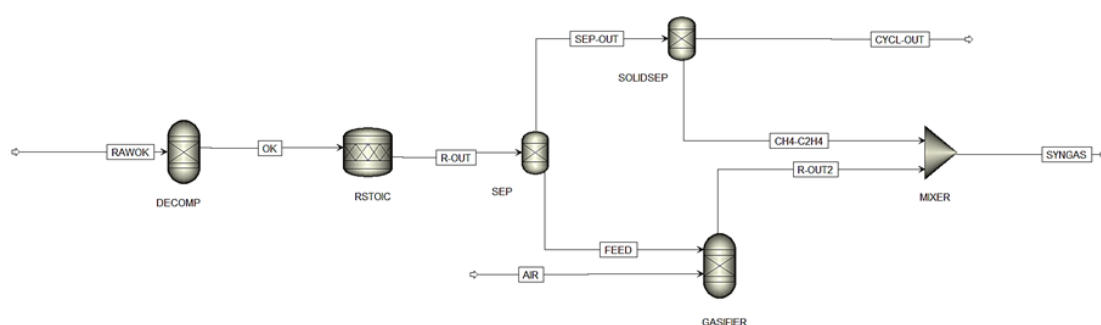


Figure 7. The flowchart used for the process simulation in Aspen Plus.

Subsequently, a stoichiometric reactor block (RStoic) was used for the estimation of CH_4 and C_2H_4 production, as they constitute the most prominent gaseous products from devolatilization reactions [57–59] (formed in the pyrolysis zone shown in Figure 6c) that cannot be directly simulated in an RGibbs block, owing to the inherent impracticalities arising from the complexity of such a system. In order to circumvent this issue and in an attempt to quantitatively assess the experimentally measured amount of methane and ethylene in the reactor effluent, their generation was simulated by considering their

formation from solid carbon and hydrogen through the reactions; $C_{(s)} + 2H_2 \rightarrow CH_4$ and $2C_{(s)} + 2H_2 \rightarrow C_2H_4$. In this regard, the redistribution of carbon and hydrogen atoms present in the original biomass via their conversion to CH_4 and C_2H_4 (as well as a very small amount of non-reactive carbon that was identified in the cyclone exit) could be estimated by means of an atom balance. Therefore, the values for the fractional conversion of carbon were calculated via a Design Spec block and were set as 10% and 5% for each reaction, respectively, in order to match the experimental contents in the produced syngas. The total flow of the produced CH_4 and C_2H_4 and the decomposed biomass (R-OUT) are then driven to a separator block (Sep), where a small fraction of char, ash and all of CH_4 and C_2H_4 are separated from the gas feed of the gasifier (stream SEP-OUT), while the rest of the gases and reactive carbon are fed to the main reactor of the process (i.e., stream FEED entering the GASIFIER block). The value for the split fraction of char was equal to 1%, calculated from the total carbon balance and according to the carbon content in the char residues. The latter was calculated from the char/ash residue post-reaction. Specifically, the total quantity at the bottom of the cyclone was weighed post-reaction and was equal to 51.9 kg, with a measured carbon content of 43.4 wt.% (analysis not shown for brevity), resulting in a net quantity of 22.5 kg of unreacted carbon.

The gasifier was modelled as an isothermal RGibbs reactor, operating at ambient pressure. The temperature of the reactor (834 °C) was set as the average temperature measured experimentally by the thermocouples at the middle of the gasifier bed zone. Crucially, the required amount of air entering the RGibbs reactor was calculated based on the molar flows of carbon and hydrogen after their partial conversion to CH_4 and C_2H_4 (also accounting for the amount of unreacted char in the bottom of the cyclone) and not on the ones contained in the as-received biomass, effectively leading to an apparent equivalence ratio of 0.30. By definition, it is evident that the latter will be slightly higher than the conventionally defined equivalence ratio which is 0.25. Lastly, olive kernel fuel, ash and unreacted carbon are separated as solids from the mixture simulating the residual solid in the bottom of the cyclone (CYCL-OUT), while the reactor outlet (R-OUT-2) is mixed with the amount of methane and ethylene in order to produce the final syngas stream.

Also, the presence of tars as well as sulphur and chlorine are neglected, given the low amount of tar compounds measured in the experiments (vide infra) and the absence of S and Cl species in the original biomass (Table 3), respectively, while traces of ammonia are formed as the only N-containing species. Indeed, according to a comprehensive review for simulating biomass gasification in terms of tar modeling [32], due to its associated complexities, such a simulation requires an elaborate and detailed methodology. However, such estimations are out of the scope of the present work.

3. Results and Discussion

3.1. Thermal/Kinetic Behavior of Olive Kernel under Air

Thermal analysis

Thermal analysis of the olive kernels was conducted under air, since thermogravimetric analysis under an oxidative atmosphere represents burning profiles and indicates the degradation route for the olive kernel fuel. The results are depicted in Figure 8, while quantification results can be seen in Table 5. Evidently, it was revealed that several weight loss profiles under an oxidative environment were attained. In particular, three different weight loss stages and peaks were resolved, subsequently attributed to moisture evaporation, oxidative degradation of volatile matter, and residual char combustion, in an ascending temperature order. This behavior is briefly discussed next.

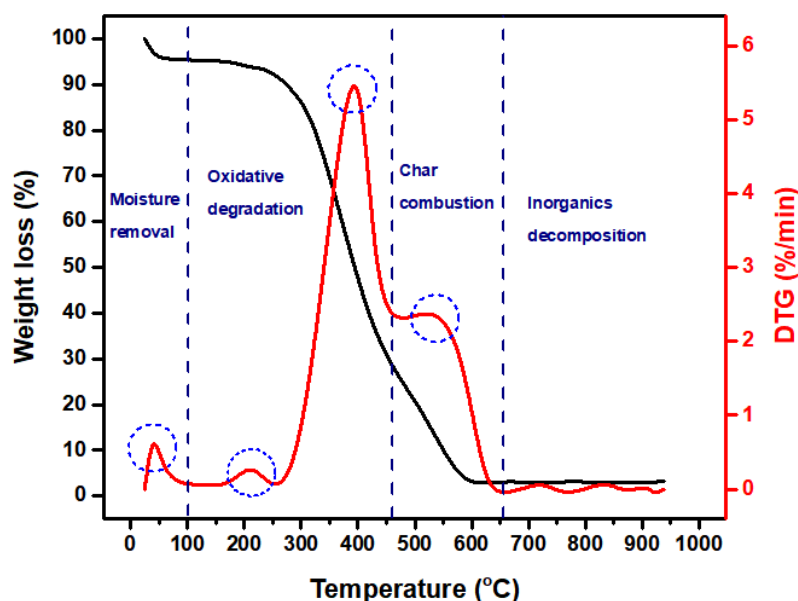


Figure 8. TG-DTG curves of thermal decomposition of olive kernel under air.

Table 5. Characteristic thermal and kinetic parameters of olive kernel under oxidative conditions (air).

Oxidative Degradation Zone				
Temperature Range (°C)	T_{peak} (°C)	Mass Loss (%)	Maximum Rate of Weight Loss (%/min)	Activation Energy Range ^a (kJ/mol)
100–460	395	70	5.6	56–110
Char Combustion Zone				
Temperature Range (°C)	T_{peak} (°C)	Mass Loss (%)	Maximum Rate of Weight Loss (%/min)	Activation Energy Range ^a (kJ/mol)
460–650	530	20	2.2	47–85

^a Based on the function of the different reaction mechanism.

In the first zone, the initial weight loss (ca. 5%) was typically ascribed to moisture evaporation at an onset temperature of 30 °C until ~110 °C. Moreover, the peaks in the second zone between 150 and 460 °C were attributed to devolatilization reactions. During this stage, a high weight loss of ca. 70% was observed, evidencing the predominance of oxidative decomposition of the volatile matter contained in the olive kernel fuel. Specifically, the main peak at around 400 °C was a direct result of the highest weight loss rate (5.7%/min) and was associated with the chemical decomposition of cellulose and lignin, while the smaller peak at around 220 °C was ascribed to both the release of residual moisture from the bulk of the solid and the decomposition of hemicellulose [27]. After the oxidative degradation and the release of volatiles, the next zone contained the combustion of char, resulting in an additional mass loss of ca. 20% (see Figure 8). Finally, two small peaks were observed at relatively high temperatures, attributed to the decomposition of the inorganic matter, the low intensity of which is in agreement with the low ash content of olive kernels.

In general, the obtained results are in good agreement with the typically high cellulose and lignin content of olive kernels (ca. 25 wt.% and 45 wt.%, respectively) [60–62]. Also, the presence of only one distinct peak associated to both cellulose and lignin decomposition indicates a complex degradation pathway for the olive kernel. It is worth mentioning that the oxidative degradation of the as-obtained olive kernels takes place at a higher temperature compared to other biomass fuels, presumably attributed to the notably higher lignin content in the former and due to the fact that lignin is generally decomposed at

higher temperatures compared to holocellulose. Notably, an overlap was seen between the second and third zone. Indeed, it is known in the literature that upon exposure of the char surface to reactive oxygen species, the processes of char oxidation and devolatilization reactions may take place indistinguishably, effectively leading to the presence of a shoulder peak [53,60,62,63]. In addition, the mass loss observed during degradation and combustion is in good agreement with the volatile matter and carbon content of typical olive kernel biomass fuels [64,65].

Kinetic analysis

Kinetics of non-isothermal thermogravimetric analysis were conducted in order to kinetically evaluate the as-received olive kernel biomass. Generally, both the activation energy and the pre-exponential factor are important design parameters for biomass gasification processes. However, it must be stated that in the present study the calculated activation energy value is not used in the process simulation, but merely for comparison purposes with other relevant lignocellulosic solid biomass fuels. Thus, complementary to the thermal behavior of the biomass fuel, a kinetic analysis in each stage was also conducted, employing the well-established Coats-Redfern method at a given heating rate. The general equation is well described in the literature and is defined as follows ((Equation (2)) [66,67];

$$\ln \left[\frac{g(a)}{T^2} \right] = \ln \left[\frac{AR}{\beta E_a} \left(1 - \frac{2RT}{E_a} \right) \right] - \frac{E_a}{RT} \quad (2)$$

Concerning the function of reaction mechanism, $g(a)$, different models describing biomass thermal decomposition were applied in the present study, as reported in relevant studies [68,69]. More importantly, it can be seen from Equation (2) that by plotting the expression $\ln[g(a)/T^2]$ as a function of the inverse absolute temperature in an Arrhenius-like plot diagram the activation energy (E_a , in kJ/mol) can be directly calculated from the slope of the linear fit curve. Table 5 summarizes the range of E_a values for both oxidative degradation and char combustion stages, by applying different reaction mechanism functions. A wide range of E_a values were attained for both stages, further confirming the complexity of the oxidative degradation reactions and residual char combustion of olive kernels. The high activation values observed in the devolatilization zone can be associated with the high volatile matter content and lignin specifically [53,63,70]. In any case, the calculated activation energy values of the olive kernels used in this work were similar to the average values of other biomass fuels such as cotton stalk, olive pomace, sugar cane bagasse and various lignocellulosic wastes [63,70].

3.2. Experimental Results

Firstly, it should be mentioned that the initial attempts to work within a range of equivalence ratio values between 0.20 and 0.30 was not achievable due to technical issues. Specifically, frequent blockages were observed, since the screw feeder practically stopped operating at times. This was directly attributed to the high density of the feedstock olive kernels (Table 3). Indeed, the operation of the existing screw feeder in the plant had been robust under operation with wood pellets with low/intermediate density values and similar biomass fuels (400–700 kg/m³). However, in the case of the specific olive kernel biomass, its high density resulted in the screw conveyor operating at its minimum capacity (i.e., in minimum mass flow), necessitating the need for manual on/off operation in order to achieve a somewhat steady flow of the solid fuel into the reactor inlet. At the same time, precisely owing to the high calorific content of the feed olive kernels (Table 3), operation of the screw feeder under increased capacity (which would result in a steady albeit higher biomass flow) would probably cause overheating of the reactor above 1000 °C due to the increased extent of combustion reactions. This condition, however, would automatically trigger the shutdown of the plant due to safety protocols. As a result, the biomass feed rate was inevitably subjected to fluctuations, a finding that was also reported in the work by Bandara et al. [38]. Moreover, the variabilities in the solid inlet flow caused a pressure

drop in the reactor pressure, leading to the backflow of syngas inside the reactor. This also resulted in the automatic shutdown of the plant, precisely due to the negative pressure gradient. In order to solve this issue, a minimal amount of pure CO₂ (ca. 6 Nm³/h) was inserted into the reactor, adequate to maintain a stable pressure above the safety limit and maintaining the one-way flow of syngas outwards the reaction unit. However, this amount of CO₂ was equal to less than 1% of the air inlet flow, thus disregarded as a gasifying agent and considered an inert gas that did not contribute to the overall mass balances. All things considered, the unit could eventually maintain a quasi-steady-state operation for 12 h at an average feeding rate of ~600 kg/h, leading to a value of ER around 0.25 ± 0.03 and the obtained experimental results are presented below.

Firstly, the average temperature of the gasification process along the height of the gasifier and at the outlet is shown in Figure 9. Taking into consideration that both the pre-heated air and olive kernels were inserted at the bottom of the reactor, the maximum temperature was observed in the bed zone (where combustion reactions take place) and was equal to 834 °C. Isothermal conditions were established along the freeboard zone of the reactor.

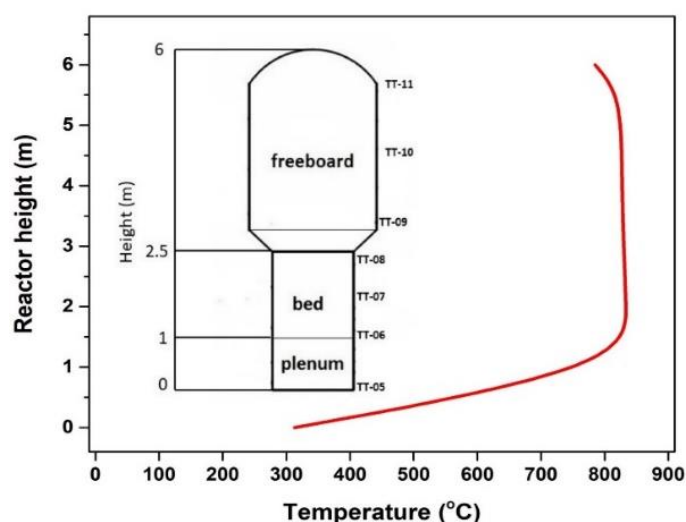


Figure 9. Temperature profile of the gasifier.

As for syngas composition, the average values of volume fractions (associated with an experimental relative error of 5%) are collectively shown in Table 6. The heating value of syngas was calculated by Equation (3) and was validated by a separate simulation of the stream in Aspen Plus. Furthermore, the cold gas efficiency of the process was calculated by Equation (4). Despite the aforementioned issues towards reaching a steady-state operation, the reactor outlet gas composition was continuously monitored in-line via a μ -GC (Table 6). It was observed that the air-blown gasification of the olive kernel biomass resulted in a rich-CO₂/CO syngas composition (18.9 vol.% and 17.1 vol.%, respectively), followed by hydrogen production (13.5 vol.%). Additionally, methane concentration was ca. 4 vol.%, whereas minor quantities of hydrocarbons were detected (less than 1.6 vol.%).

Table 6. Composition (% v/v) and LHV of the experimentally produced syngas.

H ₂	CO	CO ₂	N ₂	CH ₄	C ₂ H ₄	C ₂ H ₆	LHV (MJ/Nm ³)	LHV (MJ/kg)	H ₂ /CO
13.5	17.1	18.9	44.7	4.2	1.1	<0.1	5.74	5.00	0.79
C ₂ H ₂	C ₃ H ₈	C ₄ H ₁₀	C ₅ H ₁₂	C ₆ H ₁₄	C ₆ H ₆	C ₇ H ₈			
<0.1	<0.2	trace	trace	trace	0.05	n.d.			

n.d.: not detected.

It should be clarified at this point that tar content during the gasification test was not fully quantified based on a standardized measurement protocol (e.g., “CEN/TS 15439: 2006). However, two substances that are considered as major tar compounds [38], namely benzene and toluene were monitored in the μ -GC. In this regard, even though benzene cannot be technically considered as a tar compound, it was included in the measurements as a semi-quantitative estimation of tar content, since its concentration is typically higher compared to other tar compounds by an order of magnitude. Notably, a minimal quantity of benzene (500 ppm) and non-detectable amounts of toluene were detected, possibly indicative of the beneficial role of bauxite and oxidative reaction environment on tar cracking [32,58].

According to relevant studies [71], the quantity of the major tar components during an air-blown biomass BFB gasification can vary widely, between 1–40 g/Nm³). To the best of our knowledge, an optimized gasification process, through appropriate selection of operating parameters (temperature, gasification agent, equivalent ratio or steam-to-biomass ratio and residence time) allow for the production of a considerably cleaner product gas. Moreover, physical treatments, which include dry and wet cleaning processes, are associated with tar removal efficiencies of up to 99%, albeit disadvantageous in terms of potentially reducing energy conversion efficiency and generating highly hazardous waste materials. In any case, the precise tar measurement and further syngas clean-up was out of the scope of the present work.

Concerning the calorific content of the synthesis gas produced, not unexpectedly, a relatively moderate heating value was calculated (i.e., 5.75 MJ/Nm³) due to the employment of air as the gasifying agent, thus the produced syngas can be considered as a suitable engine fuel. However, considering indicative values of LHV in other studies examining biomass air gasification, the value calculated herein lies on the highest end of the reported values [26,28,29,38,43]. Lastly, the cold gas efficiency (CGE) was calculated by Equation (4) through the nitrogen balance and from the average inlet air flow, i.e., approximately 33.9 kmol/h. Intriguingly, its value was found to be 87.4%, which is notably high compared to other literature studies [38,41–43] investigating biomass gasification in air-blown BFB reactors. This is mostly attributed to the uncertainties in the N₂ content in the reactor outlet as well as the fluctuations in the syngas flow rate, both stemming from the variabilities in the biomass feeding rate. Therefore, this metric cannot be considered as a quantitative validating factor for the experimental results, precisely owing to its exceedingly high and practically unrealistic value.

Furthermore, a comparison of the present results with previous research exploring the gasification of similar olive pit/kernel and typical woody biomass fuels at a similar scale [26,28,57–59,72] is shown in Table S2. It can be seen that H₂ and CO concentrations in this work are relatively lower, whereas CO₂ content was significantly higher, indicating the uncertainties and difficulties of scaling-up a biomass gasification plant. This last observation can be presumably ascribed to two key operational factors. On the one hand, the somewhat intermittent biomass flow could have led to a temporary operation under a rather high ER value. This would probably result in a greater extent of combustion/oxidation reactions that increase CO₂ concentration at the expense of H₂ and CO [54,59]. On the other hand, it can be postulated that the presence of bauxite as the bed material exerted a dual effect in the process, not only due to its role in enhanced tar cracking, but also due to its high oxygen transport. Indeed, it has been reported that bauxite is associated with a significant transfer capability of oxygen species from its structure [46,48,49], which can readily and fully oxidize carbon and hydrogen species in their vicinity in a fluidized bed. So, this may result in a rather high yield of CO₂ coupled to a decrease in H₂ yield, further confirming the increased CO₂ formation during the experimental tests, as well as the differences between the simulation results (see below). In any case, these differences do not significantly affect the calorific content of the produced syngas, as the LHV values varied only slightly, between 4.5 and 5.9 MJ/Nm³.

$$\text{LHV}(\text{MJ}/\text{Nm}^3) = \frac{([\text{CO}] \times 126.36 + [\text{H}_2] \times 107.98 + [\text{CH}_4] \times 358.18 + [\text{C}_2\text{H}_4] \times 592.50)}{1000} \quad (3)$$

where i is the molar fraction of the syngas component ($i = \text{CO}, \text{H}_2, \text{CH}_4$ and C_2H_4).

$$\text{CGE}(\%) = \frac{\text{LHV}_{\text{syngas}}(\text{MJ}/\text{Nm}^3) \cdot \text{Syngas flow}(\text{Nm}^3/\text{h})}{\text{LHV}_{\text{biomass}}(\text{MJ}/\text{kg}) \cdot \text{Biomass flow}(\text{kg}/\text{h})} \cdot 100 \quad (4)$$

3.3. Simulation Results

3.3.1. Experimental vs. Simulation Results

Next, the results from the simulation study are discussed and compared with the results from the gasification experiments. It should be stated that the comparison is made on the basis of the same equivalence ratio (i.e., 0.25), which is the average value for the experimental results and one that corresponds to an apparent equivalence ratio (as introduced herein) of 0.30 in the simulation study. Indeed, as can be comparatively seen in Figure 10, the simulation of the process generally agreed with the experimental values, indicating the ability of the employed model in predicting the behavior of the feed biomass under realistic conditions. More specifically, the simulated values for CO, CH₄ and C₂H₄ were very close. However, a discrepancy exists between H₂ and CO₂ contents, as the theoretical model resulted in an overestimation and an underestimation, respectively. Intriguingly, even with these differences, the overall heating value of the generated syngas was practically identical in both cases. The above can be attributed to the presence of bauxite, as briefly stated above. Due to its significant oxygen transfer capability, bauxite can probably affect the composition of the produced syngas leading to a CO₂-rich syngas production. At the same time, the increased availability of reactive and labile oxygen species due to the presence of bauxite can also lead to a consumption of hydrogen species as well, through their oxidation towards water, as has been reported elsewhere [47,49]. Nonetheless, the adverse effect of oxygen transport on diminished H₂ concentration can be compensated for by its prominent tar cracking and water-gas shift performance (WGS, Equation (5)).

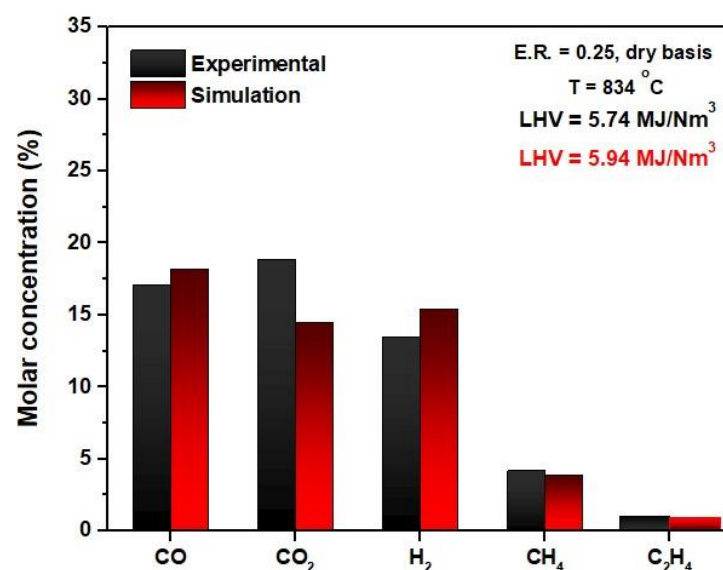


Figure 10. Comparison of the simulation and experimental results at E.R. = 0.25.

Also, the lower heating value of the produced syngas was found to be similar to the experimental value (i.e., $\sim 5.94 \text{ MJ/Nm}^3$), further showcasing the good agreement between the experimental and simulation results.

The complex phenomena described so far cannot be practically simulated with very high accuracy with the use of a simple thermodynamic equilibrium as the one used in this work. Indeed, the employment of an RGibbs reactor is generally associated with an underestimation of CO_2 and CH_4 and an overestimation of H_2 and CO [32]. In order to account for all the variabilities in syngas composition between the two datasets, the validation of the simulation model was assessed by employing the statistical metric of the root mean square (RMS) (Equation (6)). Indeed, RMS is a widely established data analysis indicator in relevant studies comparing experimental and theoretical biomass gasification results [73]. In this regard, the RMS value in the present work was equal to 2.62, which is relatively low compared to the values reported in the aforementioned works [73–77]. Ergo, the employed methodology for the simulation of the process can be considered valid enough, even accounting for the aforementioned uncertainties.

$$\text{RMS} = \sqrt{\frac{\sum_{i=1}^N (y_{i,\text{exp}} - y_{i,\text{sim}})^2}{N}} \quad (6)$$

where, y_{exp} and y_{sim} is the experimental and simulated syngas composition (in vol.%), respectively, I refers to the syngas component (i : H_2 , CO , CO_2 , CH_4 and C_2H_4) and N is the number of components.

Lastly and as a further means of comparison, the cold gas efficiency was also calculated from the simulation results and was found equal to 78.0%. This value was lower than the respective value for the experimental results; however, it was considered more valid by accounting for the uncertainties in the experimental results. In any case, this was considered a notably high CGE value and was attributed to the relatively high LHV value of the generated syngas and/or the enhanced tar cracking capability of bauxite in the fluidized bed (vide supra).

In light of the above, the variations in key properties, i.e., syngas composition, syngas LHV and CGE, was next explored in a further simulation study by examining the effect of relevant process parameters with the scope of gaining preliminary insight for the design of future experiments. More specifically and given the scale of the plant, it was deemed appropriate to assess the effect of parameters that;

- are not cost-intensive and can be realistically applied in the unit with minor modifications,
- are not expected to induce significant changes in the reactor and combustion chamber temperatures, eliminating the need for changes in the safety protocols,
- can be meaningfully evaluated via the simulation methodology used herein.

In this regard, it must be noted that the effect of gasification temperature was omitted in the present study, since it is practically a dependent variable in a gasification plant and cannot be effectively controlled. As stated elsewhere [32,59], higher ER values are expected to lead to higher reactor temperatures, thus favoring the progression of exothermic reactions which generate CO_2 and CH_4 . On the contrary, a high moisture content in the biomass may lead to a temperature decrease inside the reactor, due to the high latent heat of water vaporization and the increased extent of endothermic reactions favoring CO and H_2 generation [78–80]. Furthermore, the simulation of the gasifier in the present model was realized collectively via a single RGibbs block that was not able to distinguish between combustion (exothermic) and reforming (endothermic) reactions at the axial direction. Thus, its operating temperature was set in all cases as the average temperature in the bed, i.e., $834 \text{ }^\circ\text{C}$. As for the CH_4 and C_2H_4 contents in the final syngas, they were expected to be somewhat constant under the examined cases [54,55,81], so the simulation regarding their formation remained unaltered.

Therefore, the examined scenarios involved the gasification of olive kernels under the following conditions;

- Air gasification of the as-received olive kernels with variable apparent equivalence ratios. In practice, this scenario involved alterations only in the biomass feeding system of the unit; specifically, replacement of the existing screw feeder with an apparatus able to handle lower mass flows of the existing olive kernel.
- Pre-treatment of biomass via drying prior to gasification. In this case, the high moisture content in the original olive kernels was largely reduced by means of a single air-drying step applied in situ in the plant without the need for external heat provision, leading to a residual H₂O content of as low as 3 wt.%.

3.3.2. Effect of Equivalence Ratio

As mentioned above, the design of the existing feeding system along with the properties of olive kernels led to fluctuations in the feeding rate. For this reason, the results from the simulation model were used to better predict the effect of ER in the quality of the produced syngas. Figure 11a shows a remarkable decrease for CO and H₂ concentrations at higher air/biomass ratios, while an upward trend in CO₂ content is seen upon an increase in the ER values. As mentioned before, increased air flow in the reactor favors the oxidation reactions, increasing CO₂ concentration at the expense of CO and H₂ [54,55,81]. In particular, within the examined ER range, the volumetric carbon monoxide and hydrogen fraction (on a dry basis) decreased from 22.7% to 7.4% and from 26.2% to 8.4%, respectively, while CO₂ volume fraction was increased from 11.1% to 19.2%. Notably, the alterations of ER resulted in an almost constant H₂/CO ratio of 0.82. Also, as seen in Figure 11b, the LHV of dry syngas notably decreased with increasing ER, due to both the decrease in H₂+CO content and the more prominent dilution due to the increased nitrogen fraction. Also, CGE is strongly dependent on the LHV, since it is defined as the ratio of the energy input and the potential energy output based on the LHV of both the solid fuel and syngas [54,55,81] and thus presents a descending trend. These tendencies in the gasification parameters are in good agreement with other relevant works [54,55,81–87].

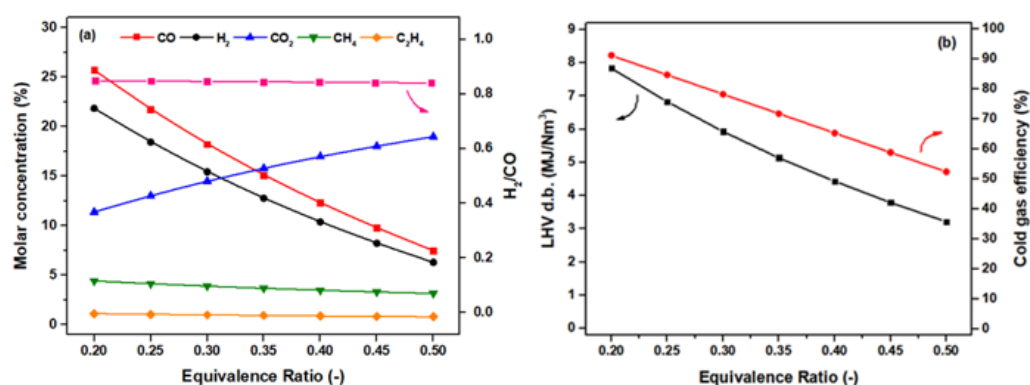


Figure 11. Effect of equivalence ratio on syngas composition (a) and on LHV (dry basis) and cold gas efficiency (b). Reaction temperature = 834 °C.

3.3.3. Effect of Biomass Drying

As reported in the literature [54,59,88], the biomass moisture content remarkably affects the overall gasification reactions network, because water vaporization inside the reactor absorbs heat, in turn leading to a decrease in the reactor temperature. Moreover, the produced steam is able to react with other compounds during all stages of the gasification process. The effect of residual moisture content on syngas composition and gasification efficiency is depicted in Figure 12. It must be noted that the moisture content was varied over a realistic range (3–18% on a mass basis), taking into consideration the efficiency of the existing and applicable drying technologies. As for syngas composition (Figure 12a),

it was observed that a progressive decrease in residual moisture led to a decrease in both the H₂ and CO₂ volume fractions (on a dry basis), from 15.5% to 12.8% and from 14.6% to 11.8%, respectively. On the contrary, an increase in CO fraction from 18.1% to 21.9% upon decrease in moisture was observed. These findings can be attributed to the significant role of water in the extended reaction network that takes place in a gasifier. More specifically, a higher moisture content favors the reactions involving H₂O (Equations (7)–(9)) and the WGS reaction especially (Equation (5)). These differences in H₂ and CO production are also reflected in the H₂/CO ratio, which is decreased with reducing moisture content. Therefore, syngas quality and its possible exploitation in several downstream processes is also affected.

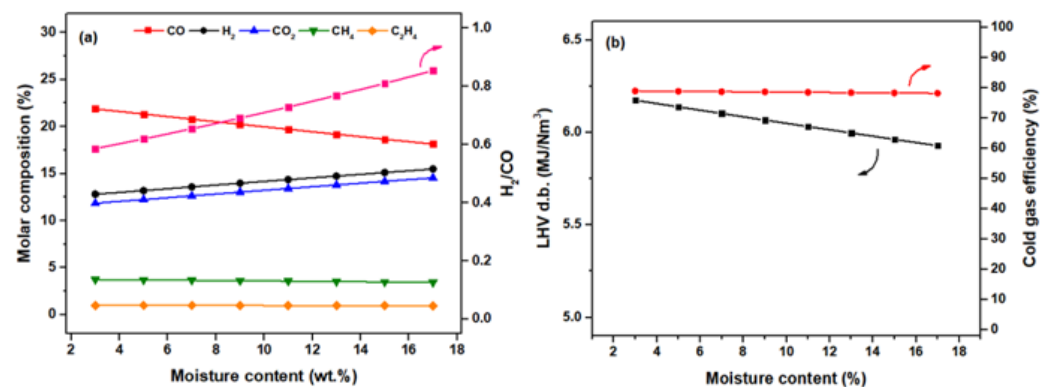
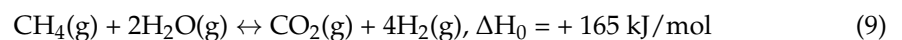
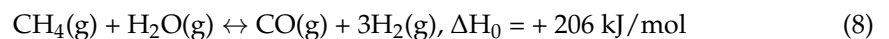


Figure 12. Effect of residual biomass moisture on syngas composition (a) and LHV (dry basis) and cold gas efficiency (b). Reaction temperature = 834 °C.

Lastly, a negligible effect of moisture content was observed in the case of CH₄ and C₂H₄, since their production was kept constant based on the experimental results. This can be also confirmed by several relevant reports highlighting the insignificant effect of moisture content in the generation of CH₄ and other light hydrocarbons [54]. Furthermore, the effect of biomass moisture content on the gasification performance parameters is depicted in Figure 12b. The syngas LHV value slightly increased with the decrease of moisture content, from 5.9 to 6.2 MJ/Nm³, owing to the monotonic increase in CO formation. As for the cold gas efficiency, CGE value remained practically constant. This was due to the fact that although the syngas LHV value increased slightly, the lower moisture content in syngas resulted in a lower mass flow, leading to a practically constant ratio (see Equation (4)). From a practical point of view, significantly higher heat would be required in the gasifier for an increased water concentration in the original biomass, in conjunction with the latent heat of conversion of liquid water into superheated steam. Therefore, since a biomass fuel with higher moisture can affect the generated synthesis gas, the gasification performance and lead to increased energy consumption, the pre-treatment of the as-received biomass via a drying step should be considered from an optimization standpoint, after accounting for the energy penalty imposed from drying itself.

3.4. Syngas Exploitation for District Heating

Motivated by the largely successful operation of the plant and along with the effectiveness of the proposed simulation methodology, a brief assessment of the possible syngas exploitation for district heating (DH) purposes was next attempted. Although the conventional DH processes are essentially part of a combined heat and power (CHP) plant, the implementation of CHP would require the additional installment of an electric generator, therefore this scenario is not considered herein. Thus, it was assumed that generation of

DH-grade steam could be facily realized via combustion of the generated syngas in the existing combustion chamber after the exit of the cyclone. Elsewhere, this exploitation pathway for syngas generated from biomass gasification has been suggested [89–91].

Specifically, using simulation data under a steady-state operation, an estimation of the generation of exploitable heat can be made. More specifically, by considering the obtained syngas flow rate and lower heating value and by assuming a typical boiler efficiency of 0.85, the thermal output of the process can be estimated at around 1.61 MWth, or 7.0 GWh for a continuous six-month operation. This heat can be potentially used to cover the heating needs of around 700 households in the nearby village of Aoiz (Figure 5) with a 2018 population of 2634, effectively rendering the plant a dedicated biomass-fueled district heating station with minimal losses due to the proximity between the plant and the end-users.

4. Conclusions and Outlooks

A large-scale and bauxite-assisted olive kernel air BFB gasification was thoroughly examined at a 2 MWth gasification plant in CENER facilities at Navarra, Spain. Discontinuous feeding of biomass led to a 12 h operation at an average value of $ER = 0.25 \pm 0.03$. Experimental results demonstrated a CO₂-rich syngas production with a typical heating value of $LHV = 5.74 \text{ MJ/Nm}^3$. In addition, the beneficial role of bauxite towards complete tar elimination was confirmed by the absence of detectable tar compounds at the reactor outlet.

The simulation of the process was next attempted via a proposed methodology in Aspen Plus utilizing experimental data. Intriguingly, a good agreement between the experimental and simulation results was attained, as affirmed by the root mean square value, indicating the validity of the model proposed in this work.

In this regard, simulations were conducted in order to examine the potential operation of the plant under potential varying gasification conditions by using the same biomass feedstock.

In specific, variations in key process parameters that can be easily implemented in the existing plant, namely variations in the equivalence ratio and the pre-drying degree of the as-received olive kernel biomass, affected syngas quality and gasification performance. Lastly, the LHV of the produced syngas production was equal to 5.94 MJ/Nm^3 and a thermal output of 1.61 MWth. This heat could be potentially used to cover the heating needs of the nearby village of Aoiz, effectively rendering the plant a dedicated biomass-fueled district heating station.

In light of the above, future test experiments are being planned for the pilot plant under different main process parameters with regards to optimizing gasification conditions and attaining the generation of a high-quality synthesis gas with minimal contaminating compounds. Furthermore, projected experiments tests are planned in order to evaluate the behavior of the gasifier using different olive-based biomass feeds with variable densities compared to the one used herein. For these tests, a recalibration of the screw conveyor will be required for the proper evaluation of the exact biomass feed flow rate.

Collectively, it should be underlined that further theoretical analysis of the process can be made by examining other scenarios that can be implemented in a gasification plant (both experimental and theoretical) but were not employed in the present work, namely co-gasification with steam and/or gasification under an oxygen-enriched air atmosphere. Indeed, steam is a cost-effective and well-known gasification agent that is widely used in several biomass gasification processes leading to enhanced H₂/CO ratios, while oxygen or oxygen-enriched gasification is associated with a diminished diluting effect of nitrogen and thereby higher heating values of syngas. Nonetheless, the addition of steam and/or oxygen enrichment will inevitably lead to significant variations in the gasifier temperature as well as in CH₄/C₂H₄ composition, which cannot be simulated by the procedure followed herein and thus requires more detailed theoretical studies.

Lastly, given the fact that the generated syngas is characterized by a typically low LHV, a potential enhancement of its calorific content can be materialized by means of integration of the already existing gasification plant with a RES-powered water electrolysis system. In this way, the produced oxygen can be directly fed to the reactor for oxygen (or oxygen-enriched) gasification of biomass and hydrogen can be blended with the reactor outlet. Collectively, the final syngas stream will be associated with a significantly high heating value and a more favorable H_2/CO for downstream Fischer-Tropsch processes, due to both the decreased nitrogen content and the increase in hydrogen content. However, a preliminary techno-economic analysis is definitely required, in order to assess the feasibility of such a scheme.

Supplementary Materials: The following supporting information can be downloaded at: <https://www.mdpi.com/article/10.3390/pr10102020/s1>, Figure S1: Particle size distribution of the as-received olive kernel for particles smaller (a) and larger (b) than 3.15 mm, Table S1: Composition and physicochemical properties of the bauxite used as bed material in the experiments, Table S2: Results of relevant studies exploring gasification of olive pits/kernels and typical woody biomass.

Author Contributions: A.L., G.V., I.G.Z. and R.P.-V. contributed to gasification studies and fuel characterization; Y.F. and N.N. contributed to project administration and funding acquisition. Finally, all authors reviewed and edited the manuscript prior to submission, while A.L. submitted the manuscript in its final form. All authors have read and agreed to the published version of the manuscript.

Funding: This research has received funding from the European Union's Horizon 2020 research and innovation programme under grant agreement No. 731101 (BRISK II project: Biofuels Research Infrastructure for Sharing Knowledge II). Also, this research has been co-financed by the European Union and Greek national funds through the Operational Program Competitiveness, Entrepreneurship and Innovation, under the call ERA-NETS 2018 (project code: T8EPA2-00005).

Data Availability Statement: Not applicable.

Acknowledgments: The authors acknowledge the National Renewable Energy Centre of Spain (CENER) for the excellent scientific collaboration and for providing the know-how and the facilities in Navarra, Spain for conducting the experiments in a 2 MWth scale.

Conflicts of Interest: The authors declare no conflict of interest.

References

1. International Energy Agency. Global Energy Review 2019. *Glob. Energy Rev.* **2020**. Available online: https://www.oecd-ilibrary.org/energy/global-energy-review-2019_90c8c125-en (accessed on 30 August 2022). [CrossRef]
2. European Commission. Europe's 2030 Climate and Energy Targets/Research and Innovation Actions. 2021. Available online: <https://op.europa.eu/en/publication-detail/-/publication/1c8ab88a-e44d-11eb-895a-01aa75ed71a1> (accessed on 30 August 2022). [CrossRef]
3. Pelkmans Luc, I.B.T. IEA Bioenergy Countries' Report—Update 2021. Implementation of Bioenergy in the IEA Bioenergy Member Countries. 2021. Available online: <https://www.ieabioenergy.com/blog/publications/iea-bioenergy-countries-report-update-2021/> (accessed on 25 July 2022).
4. Ramos, J.S.; Ferreira, A.F. Techno-economic analysis and life cycle assessment of olive and wine industry co-products valorisation. *Renew. Sustain. Energy Rev.* **2022**, *155*, 111929. [CrossRef]
5. Puig-Gamero, M.; Parascanu, M.M.; Sánchez, P.; Sanchez-Silva, L. Olive pomace versus natural gas for methanol production: A life cycle assessment. *Environ. Sci. Pollut. Res.* **2021**, *28*, 30335–30350. [CrossRef] [PubMed]
6. Parascanu, M.M.; Puig Gamero, M.; Sánchez, P.; Soreanu, G.; Valverde, J.L.; Sanchez-Silva, L. Life cycle assessment of olive pomace valorisation through pyrolysis. *Renew. Energy* **2018**, *122*, 589–601. [CrossRef]
7. Duman, A.K.; Özgen, G.Ö.; Üçtuğ, F.G. Environmental life cycle assessment of olive pomace utilization in Turkey. *Sustain. Prod. Consum.* **2020**, *22*, 126–137. [CrossRef]
8. Di Giuliano, A.; Funcia, I.; Pérez-Vega, R.; Gil, J.; Gallucci, K. Novel application of pretreatment and diagnostic method using dynamic pressure fluctuations to resolve and detect issues related to biogenic residue ash in chemical looping gasification. *Processes* **2020**, *8*, 1137. [CrossRef]
9. IEA Net Zero by 2050: A Roadmap for the Global Energy Sector. *Int. Energy Agency* **2021**, 224. Available online: https://unfccc.int/documents/278467?gclid=EAJalQobChMIqjZkPjP-gIVidWWCh3fwA_XEAAYASAAEgL_D_D_BwE (accessed on 4 September 2022).

10. Bioelectricity—Bioenergy Europe. Available online: <https://bioenergyeurope.org/article/307-bioelectricity-2.html> (accessed on 4 September 2022).
11. Aravani, V.P.; Sun, H.; Yang, Z.; Liu, G.; Wang, W.; Anagnostopoulos, G.; Syriopoulos, G.; Charisiou, N.D.; Goula, M.A.; Kornaros, M.; et al. Agricultural and livestock sector's residues in Greece & China: Comparative qualitative and quantitative characterization for assessing their potential for biogas production. *Renew. Sustain. Energy Rev.* **2022**, *154*, 111821. [[CrossRef](#)]
12. Vourdoubas, J. Use of Renewable Energy Sources for Energy Generation in Rural Areas in the Island of Crete, Greece. *Eur. J. Environ. Earth Sci.* **2020**, *1*, 1–7. [[CrossRef](#)]
13. Vourdoubas, J. Description and Assessment of a Small Renewable Energy Community in the Island of Crete, Greece. *Open J. Energy Effic.* **2017**, *6*, 97–111. [[CrossRef](#)]
14. Alatzas, S.; Moustakas, K.; Malamis, D.; Vakalis, S. Biomass potential from agricultural waste for energetic utilization in Greece. *Energies* **2019**, *12*, 1095. [[CrossRef](#)]
15. del Mar Contreras, M.; Romero, I.; Moya, M.; Castro, E. Olive-derived biomass as a renewable source of value-added products. *Process Biochem.* **2020**, *97*, 43–56. [[CrossRef](#)]
16. Aguado, R.; Vera, D.; López-García, D.A.; Torreglosa, J.P.; Jurado, F. Techno-economic assessment of a gasification plant for distributed cogeneration in the agrifood sector. *Appl. Sci.* **2021**, *11*, 660. [[CrossRef](#)]
17. Christoforou, E.; Fokaides, P.A. A review of olive mill solid wastes to energy utilization techniques. *Waste Manag.* **2016**, *49*, 346–363. [[CrossRef](#)]
18. Ongen, A.; Ozgu, C.; Ayol, A. Biomass gasification for sustainable energy production: A review. *Int. J. Hydrog. Energy* **2022**, *47*, 15419–15433. [[CrossRef](#)]
19. Narnaware, S.L.; Panwar, N.L. Biomass gasification for climate change mitigation and policy framework in India: A review. *Bioresour. Technol. Rep.* **2022**, *17*, 100892. [[CrossRef](#)]
20. Ren, S.; Feng, X.; Wang, Y. Emergy evaluation of the integrated gasification combined cycle power generation systems with a carbon capture system. *Renew. Sustain. Energy Rev.* **2021**, *147*, 111208. [[CrossRef](#)]
21. Allesina, G.; Pedrazzi, S. Barriers to success: A technical review on the limits and possible future roles of small scale gasifiers. *Energies* **2021**, *14*, 6711. [[CrossRef](#)]
22. Motta, I.L.; Miranda, N.T.; Maciel Filho, R.; Wolf Maciel, M.R. Biomass gasification in fluidized beds: A review of biomass moisture content and operating pressure effects. *Renew. Sustain. Energy Rev.* **2018**, *94*, 998–1023. [[CrossRef](#)]
23. Pala, L.P.R.; Wang, Q.; Kolb, G.; Hessel, V. Steam gasification of biomass with subsequent syngas adjustment using shift reaction for syngas production: An Aspen Plus model. *Renew. Energy* **2017**, *101*, 484–492. [[CrossRef](#)]
24. Marcantonio, V.; Ferrario, A.M.; Di Carlo, A.; Del Zotto, L.; Monarca, D.; Bocci, E. Biomass steam gasification: A comparison of syngas composition between a 1-d matlab kinetic model and a 0-d aspen plus quasi-equilibrium model. *Computation* **2020**, *8*, 86. [[CrossRef](#)]
25. Song, Y.; Tian, Y.; Zhou, X.; Liang, S.; Li, X.; Yang, Y.; Yuan, L. Simulation of air-steam gasification of pine sawdust in an updraft gasification system for production of hydrogen-rich producer gas. *Energy* **2021**, *226*, 120380. [[CrossRef](#)]
26. Vera, D.; De Mena, B.; Jurado, F.; Schories, G. Study of a downdraft gasifier and gas engine fuelled with olive oil industry wastes. *Appl. Therm. Eng.* **2013**, *51*, 119–129. [[CrossRef](#)]
27. Zabaniotou, A.; Rovas, D.; Monteleone, M. Management of Olive Grove Pruning and Solid Waste from Olive Oil Extraction via Thermochemical Processes. *Waste Biomass Valorization* **2015**, *6*, 831–842. [[CrossRef](#)]
28. Vera, D.; Jurado, F.; Margaritis, N.K.; Grammelis, P. Experimental and economic study of a gasification plant fuelled with olive industry wastes. *Energy Sustain. Dev.* **2014**, *23*, 247–257. [[CrossRef](#)]
29. Manara, P.; Zabaniotou, A. Indicator-based economic, environmental, and social sustainability assessment of a small gasification bioenergy system fuelled with food processing residues from the Mediterranean agro-industrial sector. *Sustain. Energy Technol. Assess.* **2014**, *8*, 159–171. [[CrossRef](#)]
30. Lampropoulos, A.; Kaklidis, N.; Athanasiou, C.; Montes-Morán, M.A.; Arenillas, A.; Menéndez, J.A.; Binas, V.D.; Konsolakis, M.; Marnellos, G.E. Effect of Olive Kernel thermal treatment (torrefaction vs. slow pyrolysis) on the physicochemical characteristics and the CO₂ or H₂O gasification performance of as-prepared biochars. *Int. J. Hydrogen Energy* **2021**, *46*, 29126–29141. [[CrossRef](#)]
31. Maisano, S.; Urbani, F.; Cipiti, F.; Freni, F.; Chiodo, V. Syngas production by BFB gasification: Experimental comparison of different biomasses. *Int. J. Hydrog. Energy* **2019**, *44*, 4414–4422. [[CrossRef](#)]
32. Ajourloo, M.; Ghodrat, M.; Scott, J.; Strezov, V. Recent advances in thermodynamic analysis of biomass gasification: A review on numerical modelling and simulation. *J. Energy Inst.* **2022**, *102*, 395–419. [[CrossRef](#)]
33. Pio, D.T.; Tarelho, L.A.C. Industrial gasification systems (>3 MWth) for bioenergy in Europe: Current status and future perspectives. *Renew. Sustain. Energy Rev.* **2021**, *145*, 111108. [[CrossRef](#)]
34. Chambon, C.L.; Karia, T.; Sandwell, P.; Hallett, J.P. Techno-economic assessment of biomass gasification-based mini-grids for productive energy applications: The case of rural India. *Renew. Energy* **2020**, *154*, 432–444. [[CrossRef](#)]
35. Situmorang, Y.A.; Zhao, Z.; Yoshida, A.; Abudula, A.; Guan, G. Small-scale biomass gasification systems for power generation (<200 kW class): A review. *Renew. Sustain. Energy Rev.* **2020**, *117*, 109486. [[CrossRef](#)]
36. Ren, J.; Cao, J.P.; Zhao, X.Y.; Yang, F.L.; Wei, X.Y. Recent advances in syngas production from biomass catalytic gasification: A critical review on reactors, catalysts, catalytic mechanisms and mathematical models. *Renew. Sustain. Energy Rev.* **2019**, *116*, 109426. [[CrossRef](#)]

37. Mishra, S.; Upadhyay, R.K. Review on biomass gasification: Gasifiers, gasifying mediums, and operational parameters. *Mater. Sci. Energy Technol.* **2021**, *4*, 329–340. [[CrossRef](#)]
38. Bandara, J.C.; Jaiswal, R.; Nielsen, H.K.; Moldestad, B.M.E.; Eikeland, M.S. Air gasification of wood chips, wood pellets and grass pellets in a bubbling fluidized bed reactor. *Energy* **2021**, *233*, 121149. [[CrossRef](#)]
39. Pio, D.T.; Tarelho, L.A.C.; Matos, M.A.A. Characteristics of the gas produced during biomass direct gasification in an autothermal pilot-scale bubbling fluidized bed reactor. *Energy* **2017**, *120*, 915–928. [[CrossRef](#)]
40. Puig-Gamero, M.; Pio, D.T.; Tarelho, L.A.C.; Sánchez, P.; Sanchez-Silva, L. Simulation of biomass gasification in bubbling fluidized bed reactor using aspen plus®. *Energy Convers. Manag.* **2021**, *235*, 113981. [[CrossRef](#)]
41. Porcu, A.; Sollai, S.; Marotto, D.; Mureddu, M.; Ferrara, F.; Pettinau, A. Techno-economic analysis of a small-scale biomass-to-energy BFB gasification-based system. *Energies* **2019**, *12*, 494. [[CrossRef](#)]
42. Park, S.J.; Son, S.H.; Kook, J.W.; Ra, H.W.; Yoon, S.J.; Mun, T.Y.; Moon, J.H.; Yoon, S.M.; Kim, J.H.; Kim, Y.K.; et al. Gasification operational characteristics of 20-tons-per-Day rice husk fluidized-bed reactor. *Renew. Energy* **2021**, *169*, 788–798. [[CrossRef](#)]
43. Sarker, S.; Bimbela, F.; Sánchez, J.L.; Nielsen, H.K. Characterization and pilot scale fluidized bed gasification of herbaceous biomass: A case study on alfalfa pellets. *Energy Convers. Manag.* **2015**, *91*, 451–458. [[CrossRef](#)]
44. Alauddin, Z.A.B.Z.; Lahijani, P.; Mohammadi, M.; Mohamed, A.R. Gasification of lignocellulosic biomass in fluidized beds for renewable energy development: A review. *Renew. Sustain. Energy Rev.* **2010**, *14*, 2852–2862. [[CrossRef](#)]
45. Ismail, T.M.; Ramos, A.; Monteiro, E.; El-Salam, M.A.; Rouboa, A. Parametric studies in the gasification agent and fluidization velocity during oxygen-enriched gasification of biomass in a pilot-scale fluidized bed: Experimental and numerical assessment. *Renew. Energy* **2020**, *147*, 2429–2439. [[CrossRef](#)]
46. Berdugo Vilches, T.; Marinkovic, J.; Seemann, M.; Thunman, H. Comparing Active Bed Materials in a Dual Fluidized Bed Biomass Gasifier: Olivine, Bauxite, Quartz-Sand, and Ilmenite. *Energy Fuels* **2016**, *30*, 4848–4857. [[CrossRef](#)]
47. Hanchate, N.; Ramani, S.; Mathpati, C.S.; Dalvi, V.H. *Biomass Gasification Using Dual Fluidized Bed Gasification Systems: A Review*; Elsevier Ltd.: Amsterdam, The Netherlands, 2021; Volume 280, ISBN 4613491031291.
48. Marinkovic, J.; Seemann, M.; Schwebel, G.L.; Thunman, H. Impact of Biomass Ash-Bauxite Bed Interactions on an Indirect Biomass Gasifier. *Energy Fuels* **2016**, *30*, 4044–4052. [[CrossRef](#)]
49. Cherukumilli, K.; Delaire, C.; Amrose, S.; Gadgil, A.J. Factors Governing the Performance of Bauxite for Fluoride Remediation of Groundwater. *Environ. Sci. Technol.* **2017**, *51*, 2321–2328. [[CrossRef](#)] [[PubMed](#)]
50. Fryda, L.; Panopoulos, K.D.; Kakaras, E. Integrated CHP with autothermal biomass gasification and SOFC-MGT. *Energy Convers. Manag.* **2008**, *49*, 281–290. [[CrossRef](#)]
51. Michailos, S.; Zabaniotou, A. Simulation of Olive Kernel Gasification in a Bubbling Fluidized Bed Pilot Scale Reactor. *J. Sustain. Bioenergy Syst.* **2012**, *2*, 145–159. [[CrossRef](#)]
52. Dhyani, V.; Bhaskar, T. A comprehensive review on the pyrolysis of lignocellulosic biomass. *Renew. Energy* **2018**, *129*, 695–716. [[CrossRef](#)]
53. Fernandez, A.; Soria, J.; Rodriguez, R.; Baeyens, J.; Mazza, G. Macro-TGA steam-assisted gasification of lignocellulosic wastes. *J. Environ. Manag.* **2019**, *233*, 626–635. [[CrossRef](#)]
54. Niu, M.; Huang, Y.; Jin, B.; Wang, X. Simulation of syngas production from municipal solid waste gasification in a bubbling fluidized bed using aspen plus. *Ind. Eng. Chem. Res.* **2013**, *52*, 14768–14775. [[CrossRef](#)]
55. Grimekis, D.; Delgado Calvo, M.A.; Panopoulos, K.; Karellas, S. Modelling of a 3 MWTH BFB gasifier in aspenplus™. *Eur. Biomass Conf. Exhib. Proc.* **2018**, *2018*, 713–721. [[CrossRef](#)]
56. Grimekis, D.T. Experimental and Modeling Investigation of Cleaning Technologies for Carbon Dioxide, Tar and Sulfur Compounds Contained in Gasification Product Gases. Ph.D. Thesis, National Technical University of Athens, Athens, Greece, 2019. [[CrossRef](#)]
57. Kim, Y.D.; Yang, C.W.; Kim, B.J.; Kim, K.S.; Lee, J.W.; Moon, J.H.; Yang, W.; Yu, T.U.; Lee, U. Do Air-blown gasification of woody biomass in a bubbling fluidized bed gasifier. *Appl. Energy* **2013**, *112*, 414–420. [[CrossRef](#)]
58. Abdoulmoumine, N.; Kulkarni, A.; Adhikari, S. Effects of temperature and equivalence ratio on pine syngas primary gases and contaminants in a bench-scale fluidized bed gasifier. *Ind. Eng. Chem. Res.* **2014**, *53*, 5767–5777. [[CrossRef](#)]
59. Monteiro, E.; Ismail, T.M.; Ramos, A.; Abd El-Salam, M.; Brito, P.; Rouboa, A. Experimental and modeling studies of Portuguese peach stone gasification on an autothermal bubbling fluidized bed pilot plant. *Energy* **2018**, *142*, 862–877. [[CrossRef](#)]
60. Volpe, R.; Zabaniotou, A.A.; Skoulou, V. Synergistic Effects between Lignin and Cellulose during Pyrolysis of Agricultural Waste. *Energy Fuels* **2018**, *32*, 8420–8430. [[CrossRef](#)]
61. Rodríguez, G.; Lama, A.; Rodríguez, R.; Jiménez, A.; Guillén, R.; Fernández-Bolaños, J. Olive stone an attractive source of bioactive and valuable compounds. *Bioresour. Technol.* **2008**, *99*, 5261–5269. [[CrossRef](#)]
62. Jahurul, M.I.; Rasul, M.G.; Chowdhury, A.A.; Ashwath, N. Biofuels production through biomass pyrolysis—A technological review. *Energies* **2012**, *5*, 4952–5001. [[CrossRef](#)]
63. Sher, F.; Iqbal, S.Z.; Liu, H.; Imran, M.; Snape, C.E. Thermal and kinetic analysis of diverse biomass fuels under different reaction environment: A way forward to renewable energy sources. *Energy Convers. Manag.* **2020**, *203*, 112266. [[CrossRef](#)]
64. Abadir, M.F.; Barakat, F.I.; Salam, N.F.A. Kinetics of Pyrolysis of Olive Kernels Kinetics of Pyrolysis of Olive Kernels. *IOSR J. Appl. Chem. (IOSR-JAC)* **2019**, *12*, 50–56. [[CrossRef](#)]

65. Manara, P.; Vamvuka, D.; Sfakiotakis, S.; Vanderghem, C.; Richel, A.; Zabaniotou, A. Mediterranean agri-food processing wastes pyrolysis after pre-treatment and recovery of precursor materials: A TGA-based kinetic modeling study. *Food Res. Int.* **2015**, *73*, 44–51. [[CrossRef](#)]
66. Roncancio, R.; Gore, J.P. CO₂ char gasification: A systematic review from 2014 to 2020. *Energy Convers. Manag. X* **2021**, *10*, 100060. [[CrossRef](#)]
67. Li, S.; Song, H.; Hu, J.; Yang, H.; Zou, J.; Zhu, Y.; Tang, Z.; Chen, H. CO₂ gasification of straw biomass and its correlation with the feedstock characteristics. *Fuel* **2021**, *297*, 120780. [[CrossRef](#)]
68. Edreis, E.M.A.; Li, X.; Luo, G.; Sharshir, S.W.; Yao, H. Kinetic analyses and synergistic effects of CO₂ co-gasification of low sulphur petroleum coke and biomass wastes. *Bioresour. Technol.* **2018**, *267*, 54–62. [[CrossRef](#)] [[PubMed](#)]
69. Kozlov, A.N.; Svishchev, D.A.; Khudiakova, G.I.; Ryzhkov, A.F. A kinetic analysis of the thermochemical conversion of solid fuels (A review). *Solid Fuel Chem.* **2017**, *51*, 205–213. [[CrossRef](#)]
70. Munir, S.; Daood, S.S.; Nimmo, W.; Cunliffe, A.M.; Gibbs, B.M. Thermal analysis and devolatilization kinetics of cotton stalk, sugar cane bagasse and shea meal under nitrogen and air atmospheres. *Bioresour. Technol.* **2009**, *100*, 1413–1418. [[CrossRef](#)]
71. Valderrama Rios, M.L.; González, A.M.; Lora, E.E.S.; Almazán del Olmo, O.A. Reduction of tar generated during biomass gasification: A review. *Biomass Bioenergy* **2018**, *108*, 345–370. [[CrossRef](#)]
72. Valdés, C.F.; Chejne, F.; Marrugo, G.; Macias, R.J.; Gómez, C.A.; Montoya, J.I.; Londoño, C.A.; De La Cruz, J.; Arenas, E. Co-gasification of sub-bituminous coal with palm kernel shell in fluidized bed coupled to a ceramic industry process. *Appl. Therm. Eng.* **2016**, *107*, 1201–1209. [[CrossRef](#)]
73. Suraj, P.; George, J.; Arun, P.; Muraleedharan, C. Theoretical and experimental feasibility study of groundnut shell gasification in a fluidized bed gasifier. *Biomass Convers. Biorefinery* **2020**, *10*, 735–742. [[CrossRef](#)]
74. Karmakar, M.K.; Datta, A.B. Generation of hydrogen rich gas through fluidized bed gasification of biomass. *Bioresour. Technol.* **2011**, *102*, 1907–1913. [[CrossRef](#)]
75. Dillibabu, V.; Lakshmanan, T.; Natarajan, E. Air and Oxygen Gasification Simulation Analysis of Sawdust. *Therm. Sci.* **2019**, *23*, 1043–1053.
76. Eri, Q.; Wu, W.; Zhao, X. Numerical investigation of the air-steam biomass gasification process based on thermodynamic equilibrium model. *Energies* **2017**, *10*, 2163. [[CrossRef](#)]
77. Rodríguez-Alejandro, D.A.; Nam, H.; Maglinao, A.L.; Capareda, S.C.; Aguilera-Alvarado, A.F. Development of a modified equilibrium model for biomass pilot-scale fluidized bed gasifier performance predictions. *Energy* **2016**, *115*, 1092–1108. [[CrossRef](#)]
78. Gu, H.; Tang, Y.; Yao, J.; Chen, F. Study on biomass gasification under various operating conditions. *J. Energy Inst.* **2019**, *92*, 1329–1336. [[CrossRef](#)]
79. Mutlu, Ö.Ç.; Zeng, T. Challenges and Opportunities of Modeling Biomass Gasification in Aspen Plus: A Review. *Chem. Eng. Technol.* **2020**, *43*, 1674–1689. [[CrossRef](#)]
80. Islam, M.W. Effect of different gasifying agents (steam, H₂O₂, oxygen, CO₂, and air) on gasification parameters. *Int. J. Hydrogen Energy* **2020**, *45*, 31760–31774. [[CrossRef](#)]
81. Borello, D.; Pantaleo, A.M.; Caucci, M.; De Caprariis, B.; De Filippis, P.; Shah, N. Modeling and experimental study of a small scale olive pomace gasifier for cogeneration: Energy and profitability analysis. *Energies* **2017**, *10*, 1930. [[CrossRef](#)]
82. Elias, A.; Boumeddane, B.; Vera, D.; Jurado, F. Gasification of olive mill solid wastes for cogeneration applications in Tizi Ouzou region: Thermo-economic assessment. *Int. J. Sustain. Energy* **2021**, *40*, 1002–1026. [[CrossRef](#)]
83. Gómez-Barea, A.; Arjona, R.; Ollero, P. Pilot-plant gasification of olive stone: A technical assessment. *Energy Fuels* **2005**, *19*, 598–605. [[CrossRef](#)]
84. Ramzan, N.; Ashraf, A.; Naveed, S.; Malik, A. Simulation of hybrid biomass gasification using Aspen plus: A comparative performance analysis for food, municipal solid and poultry waste. *Biomass Bioenergy* **2011**, *35*, 3962–3969. [[CrossRef](#)]
85. Huang, F.; Jin, S. Investigation of biomass (pine wood) gasification: Experiments and Aspen Plus simulation. *Energy Sci. Eng.* **2019**, *7*, 1178–1187. [[CrossRef](#)]
86. Damartzis, T.; Michailos, S.; Zabaniotou, A. Energetic assessment of a combined heat and power integrated biomass gasification-internal combustion engine system by using Aspen Plus®. *Fuel Process. Technol.* **2012**, *95*, 37–44. [[CrossRef](#)]
87. Begum, S.; Rasul, M.G.; Akbar, D.; Ramzan, N. Performance analysis of an integrated fixed bed gasifier model for different biomass feedstocks. *Energies* **2013**, *6*, 6508–6524. [[CrossRef](#)]
88. Tuomi, S.; Kurkela, E.; Hannula, I.; Berg, C.G. The impact of biomass drying on the efficiency of a gasification plant co-producing Fischer-Tropsch fuels and heat—A conceptual investigation. *Biomass Bioenergy* **2019**, *127*, 105272. [[CrossRef](#)]
89. Rezaei, M.; Sameti, M.; Nasiri, F. Biomass-fuelled combined heat and power: Integration in district heating and thermal-energy storage. *Clean Energy* **2021**, *5*, 44–56. [[CrossRef](#)]
90. Difs, K.; Wetterlund, E.; Trygg, L.; Söderström, M. Biomass gasification opportunities in a district heating system. *Biomass Bioenergy* **2010**, *34*, 637–651. [[CrossRef](#)]
91. Kirsanovs, V.; Blumberga, D.; Karklina, K.; Veidenbergs, I.; Rochas, C.; Vigants, E.; Vigants, G. Biomass Gasification for District Heating. *Energy Procedia* **2017**, *113*, 217–223. [[CrossRef](#)]